MICROWAVE MODEL OF A DIELECTRIC SLAB WAVEGUIDE

by

Robert Franklin German[†]

Scientific Report No. 68

November 1981

Electromagnetics Laboratory
Department of Electrical Engineering
University of Colorado
Boulder, Colorado 80309

[†]This report is based on the author's M.S. Thesis

This research was supported in part by the Army Research Office (ARO) under grant DAAG29-G-0173, monitored by Dr. J. Mink.

TABLE OF CONTENTS

LIST OF FIGURES

CHAPTER I

INTRODUCTION

With the rising popularity of fiber optic links for use in data communication systems, there is a natural desire to minimize losses in such systems [1]. The mechanisms through which loss can occur include material absorption, material scattering, cladding loss and discontinuities such as bends and splices. At the present time the splicing problem is the most formidable.

Optical fiber splicing has been examined theoretically by Marcuse [2], Rulf [3] and Neumann [4]. Experimental investigation has also been conducted by Neumann [4] , Albrecht and Neumann [5] and Bisbee [6]. Operating at optical frequencies, Bisbee only measured the loss due to various splices. Neumann and Albrecht and Neumann have been able to measure the fields outside the fiber by modelling at microwave frequencies, but have not made measurements within the dielectric. While the ability to measure fields inside a guiding structure could be used to aid splice coupler design, this ability should prove especially useful in many integrated optics applications [7]. This thesis presents an experimental technique that allows accurate magnitude and phase measurements inside and outside a dielectric slab

waveguide, the two dimensional analogue of an optical fiber [8].

Bahar [9] used a microwave model to simulate an earth-ionosphere waveguide, but Haddad [10] was the first to use a microwave model of an optical dielectric slab waveguide during his study of coupling between parallel dielectric slab waveguides and radiation from bends in slab waveguides. Dielectric material was placed between two large aluminum plates to simulate a structure having no physical varation in the y direction. Field measurements inside and outside the slab are made by inserting a probe through holes in the plates. This is the experimental technique described in this thesis.

The effect of terminating a single mode dielectric slab waveguide with truncated and angled ends will be investigated. This will include measurement of the surface wave as it travels along the angled section as well as the corresponding radiation patterns. In view of these results the effects of gaps and/or offsets between sections having truncated and angled ends will be studied.

The results of this thesis are expected to motivate future research, aid in the design of optical fiber splicing and possibly lead to the invention of new integrated optic switches, modulators, directional couplers etc.

CHAPTER II

THEORY

The two dimensional dielectric slab waveguide studied in this thesis is depicted in Fig. 1. For any structure which exhibits no physical change in the y direction, it is reasonable to assume that the fields will also be constant with respect to y. Mathematically this restriction is expressed as

$$\frac{\partial}{\partial y} = 0$$

If we assume time dependence of the form

$$e^{i\omega t}$$

Maxwells equations become

$$-\frac{\partial}{\partial z} H_y = i\omega\epsilon E_x \tag{2-1}$$

$$\frac{\partial}{\partial z} H_x - \frac{\partial}{\partial x} H_z = i\omega\epsilon E_y \tag{2-2}$$

$$\frac{\partial}{\partial x} H_y = i\omega\epsilon E_z \tag{2-3}$$

$$-\frac{\partial}{\partial z} E_y = -i\omega\mu_o H_x \tag{2-4}$$

$$\frac{\partial}{\partial z} E_x - \frac{\partial}{\partial x} E_z = -i\omega\mu_o H_y \tag{2-5}$$

$$\frac{\partial}{\partial x} E_y = -i\omega\mu_o H_z \tag{2-6}$$

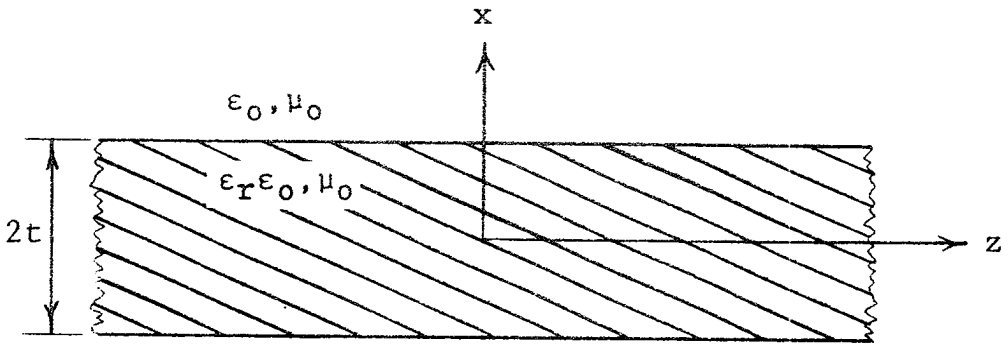

Fig. 1 Two dimensional dielectric slab waveguide.

By inspection of (2-1) through (2-6) one can see that E_y, H_x and H_z (TE polarization) are completely decoupled from E_x, E_z and H_y (TM polarization). This allows us to solve for each set of field components separately. We first examine the TE polarized field components. Once E_y is found, H_x and H_z can be determined using (2-4) and (2-6)

$$H_x = \frac{1}{i\omega\mu_o} \frac{\partial}{\partial z} E_y \tag{2-7}$$

$$H_z = \frac{-1}{i\omega\mu_o} \frac{\partial}{\partial x} E_y \tag{2-8}$$

E_y is the solution of the reduced wave equation obtained by substiuting (2-7) and (2-8) into (2-2)

$$\frac{\partial^2}{\partial z^2} E_y + \frac{\partial^2}{\partial x^2} E_y + \omega^2\mu_o\varepsilon E_y = 0 \tag{2-9}$$

If we define

$$n^2 = \varepsilon_r = \frac{\varepsilon}{\varepsilon_o}$$

and

$$k_o^2 = \omega^2\mu_o\varepsilon_o = \left(\frac{2\pi}{\lambda}\right)^2$$

(2-9) can be written

$$\frac{\partial^2}{\partial z^2} E_y + \frac{\partial^2}{\partial x^2} E_y + n^2k_o^2E_y = 0 \tag{2-10}$$

For guided waves, the symmetry of the slab waveguide in the z direction allows the following z dependence to be assumed

$$e^{-i\beta z}$$

With this (2-10) becomes

$$\frac{\partial^2}{\partial x^2} E_y + (n^2 k_o^2 - \beta^2) E_y = 0 \qquad (2\text{-}11)$$

The solution to (2-11) can be either cosinusoidal (even TE modes) or sinusoidal (odd TE modes) inside the slab and is exponentially decaying outside the slab. Such a field distribution is called a surface wave. Realizing that E_y must be continuous at the edges of the slab, the even mode solution to (2-11) is

$$E_y = A_e \cos hx \qquad |x| < t \qquad (2\text{-}12)$$

$$E_y = A_e \cos ht \; e^{-p(|x|-t)} \qquad |x| > t \qquad (2\text{-}13)$$

where

$$h^2 = n_1^2 k_o^2 - \beta^2 \qquad (2\text{-}14)$$

$$p^2 = \beta^2 - k_o^2 \qquad (2\text{-}15)$$

Substituting (2-12) and (2-13) into (2-8) yields

$$H_z = \frac{-ih}{\omega \mu_o} A_e \sin hx \qquad |x| < t \qquad (2\text{-}16)$$

$$H_z = - \frac{x \; ip}{|x| \omega \mu_o} A_e \cos ht \; e^{-p(|x|-t)} \qquad |x| > t \qquad (2\text{-}17)$$

Since H_z must also be continuous at the edges of the slab we have from (2-16) and (2-17)

$$\tan ht = \frac{p}{h} \qquad (2\text{-}18)$$

The derivation of the odd TE mode solution to (2-11) proceeds in a similar fashion yielding

$$E_y = A_e \sin hx \qquad |x| < t \qquad (2\text{-}19)$$

$$E_y = \frac{x}{|x|} A_e \sin ht \; e^{-p(|x|-t)} \qquad |x| > t \qquad (2\text{-}20)$$

$$H_z = \frac{ih}{\omega\mu_o} A_e \cos hx \qquad |x| < t \qquad (2\text{-}21)$$

$$H_z = -\frac{iP}{\omega\mu_o} A_e \sin ht \; e^{-p(|x|-t)} \qquad |x| > t \qquad (2\text{-}22)$$

$$\tan ht = -\frac{h}{p} \qquad (2\text{-}23)$$

Before we investigate the TM modes let us consider the structure that will be used to model a dielectric slab waveguide having no physical variation in the y direction. This structure is shown in Fig. 2. The surface waves described by (2-12) through (2-23) can propagate along the structure of Fig. 2 since they meet the boundary conditions of the conducting plates: there is no component of the E field tangent to the plates and the H field components are constant with respect to y. Let us now consider the TM surface waves that will have TM polarized E_x, E_z and H_y components. Because the E_x and E_z will be constant with respect to y, they can not meet the boundary conditions that tangential E fields vanish at the surface of the plates. Other types of guided waves that are composed of field components that are not

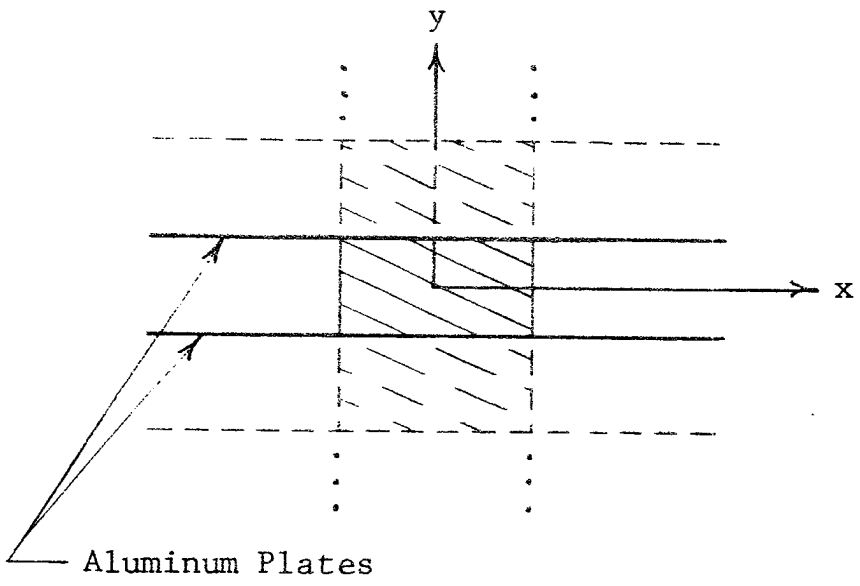

Fig. 2 Structure used to model the slab waveguide.

constant with respect to y are eliminated by choosing a plate separation (see THE MODEL) such that the higher-order TE and TM modes of the parallel plates are cutoff.

In addition to the TE surface wave modes described above there is a continuum of TE radiation modes that together are a complete solution to (2-10) and meet the boundary conditions imposed by the parallel plates. Detailed discussions of the radiation modes are presented in [8] and [11].

In order to obtain the values of h and p corresponding to the even TE modes, equations (2-14), (2-15) and (2-18) must be solved simultaneously. Substituting (2-14) and (2-15) into (2-18) yields

$$\tan ht = \frac{\sqrt{(n_1^2-1)k_o^2-h^2}}{h} \qquad (2\text{-}24)$$

which can be solved numerically. The values of h and p corresponding to the odd TE modes are found by solving the equation resulting from the substitution of (2-14) and (2-15) into (2-23)

$$\tan ht = -\frac{h}{\sqrt{(n_1^2-1)k_o^2-h^2}} \qquad (2\text{-}25)$$

Single mode operation, propagation of the first even TE mode (TE_0) only, is insured if t is chosen such that

$$t < \frac{\pi}{2k_o\sqrt{n_1^2-1}} \qquad (2\text{-}26)$$

Equation (2-26) prevents (2-25) from having a real solution thus guaranteeing that the TE_1 mode (and all higher order TE modes) will not propagate.

A quantity that is frequently used [8] in the discussion of dielectric slab waveguides is the "effective width" of the guide defined as

$$D_e = 2(t + \frac{1}{p}) \qquad (2\text{-}27)$$

A plot of effective width vs slab width is shown in Fig. 3. This plot was obtained by assuming $\varepsilon_r = 1.05$ (see SINGLE MODE DIELECTRIC SLAB WAVEGUIDE).

The fields radiated from a truncated dielectric slab waveguide are found by Lewin [12] using the Kirchhof-Huygens diffraction integral technique. A good description of this technique is presented by Marcuse [8]. If the single mode dielectric slab waveguide described above is truncated at z = 0, the electric field radiated by the end of the slab is

$$E_y(x,y) = \int_{-\infty}^{\infty} T(\mu) e^{-jk_o(\mu x + z\sqrt{1-\mu^2})} d\mu \quad z > 0 \qquad (2\text{-}28)$$

where

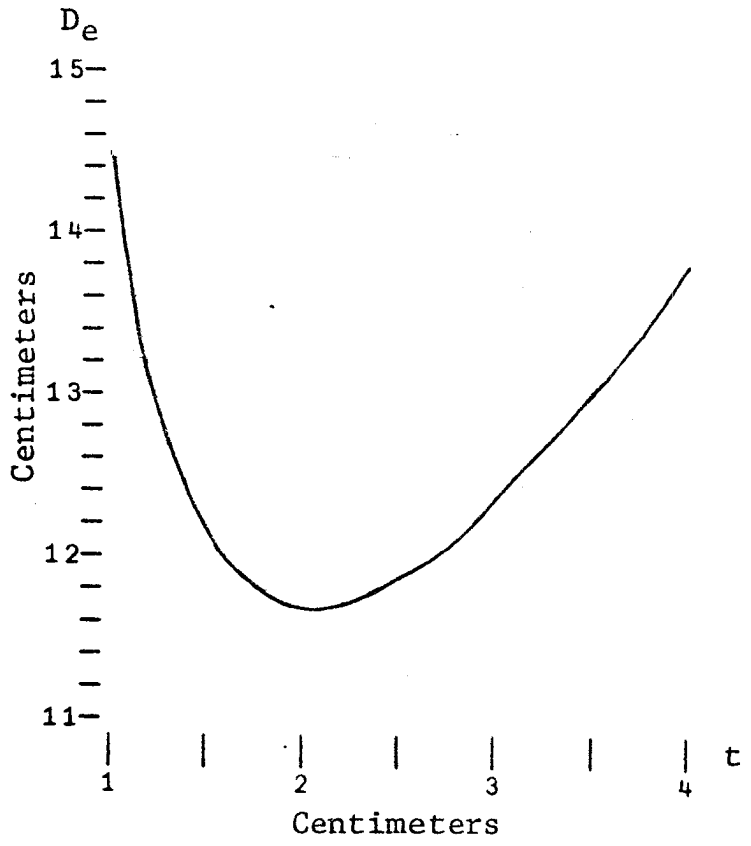

Fig. 3 Effective width of a slab waveguide.

$$T(\mu) = \frac{1}{2\pi}\int_{-\infty}^{\infty} E_y(x,0)e^{jk_o\mu x}\,(k_o dx) \qquad (2\text{-}29)$$

and

$$E_y(x,0) = \int_{-\infty}^{\infty} T(\mu)e^{-jk_o x\mu}\,d\mu \qquad (2\text{-}30)$$

To test the validity of (2-28) we set z = 0 and immediately obtain (2-30) as expected. The only other condition upon (2-28) is that it must satisfy the reduced wave equation (2-10) which can be verified by inspection. Thus (2-28) is the desired expression.

Because the incident surface wave is essentially a set of plane waves travelling in a near axial direction, the Fresnel reflection coefficient can be used to determine the magnitude of the reflected surface wave. Due to the small dielectric contrast between the slab and air, the reflected surface wave can be neglected. Under this assumption (2-12) and (2-13) can be substituted into (2-29) and simplified using (2-14), (2-15) and (2-18) to obtain

$$T(\mu) = \frac{A_e h k_o^2 \sqrt{n_1^2-1}}{\pi(p^2+k_o^2\mu^2)(h^2-k_o^2\mu^2)} \times \{p\cos(k_o t\mu) - k_o\mu \sin(k_o t\mu)\} \qquad (2\text{-}31)$$

with the corresponding radiation pattern for (2-28) being

$$F(\mu) = \frac{T(\mu)}{2}\left[\frac{\beta}{k_o} + \sqrt{1-\mu^2}\right] \qquad \mu = \sin\theta \qquad (2\text{-}32)$$

CHAPTER III

THE MODEL

To model a dielectric slab having infinite height and finite width, a piece of Sentinel extruded polyethylene foam was placed between two 240 cm by 360 cm aluminum plates as shown in Fig. 4. Selection of this foam was based upon its low dielectric constant (see Single Slab) and porousness that allowed measurements to be made within the slab. A constant field distribution between the plates was obtained by selecting a separation of 1.0 cm, the height of X-Band waveguide. Since the original thickness of the foam was 1/2 inch, a high speed band saw was required to reduce the thickness to 1 cm. Construction of the plates consisted of riveting aluminum channels to 0.2 cm thick 120 cm by 360 cm aluminum sheets. The lower plate was placed on three large tables and leveled using wooden blocks and spacers placed between the table and the plates at 44 different points. A plywood frame was attached to the upper plate (Fig. 5) allowing it to be raised and lowered by a pulley system without bending due to the force of its own weight (Fig. 6). Constant separation between the plates was maintained by placing 3/8 inch thick particle board, cut into 5 cm wide strips of various lengths, at locations where low field levels were anticipated.

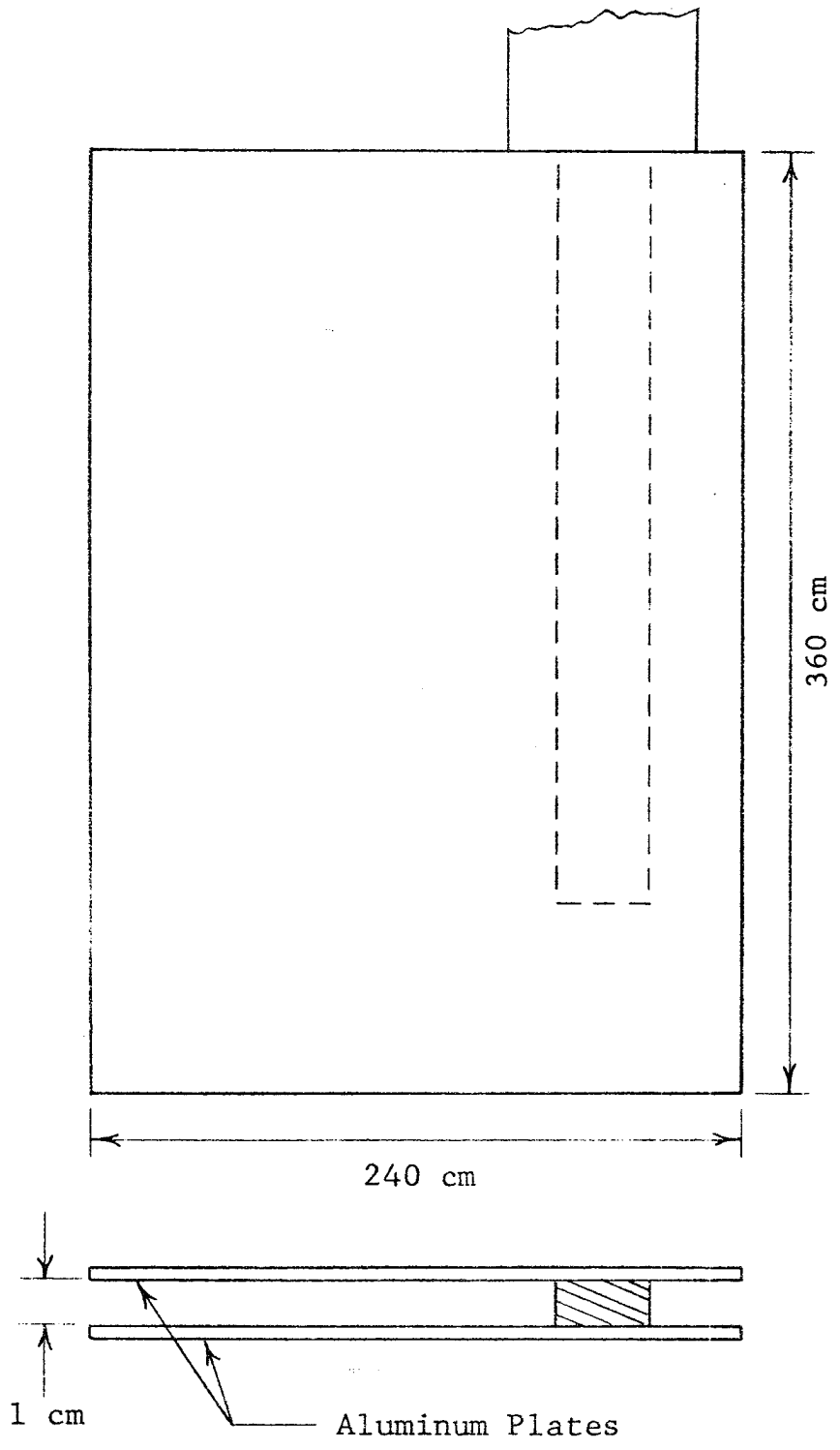

Fig. 4 Foam placed between aluminum plates.

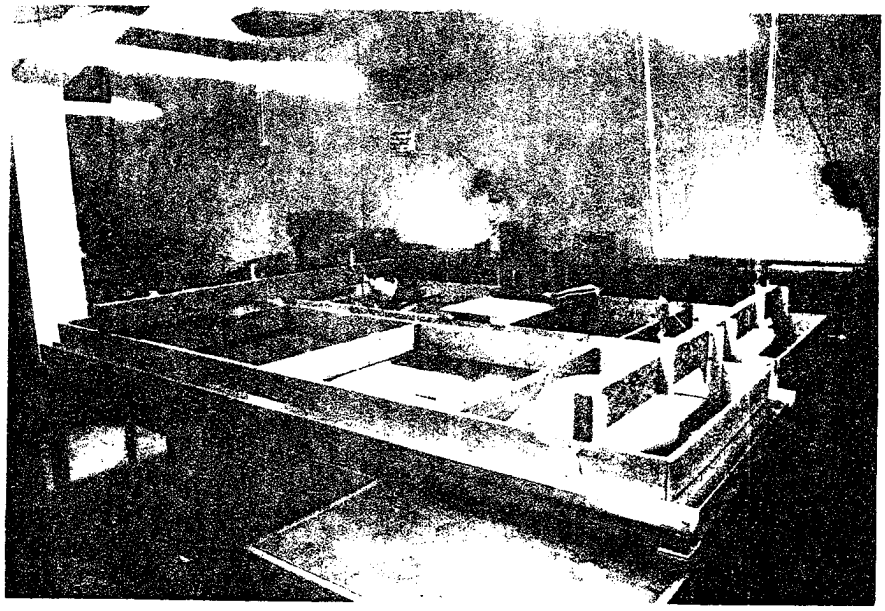

Fig. 5 Plywood frame attached to upper plate.

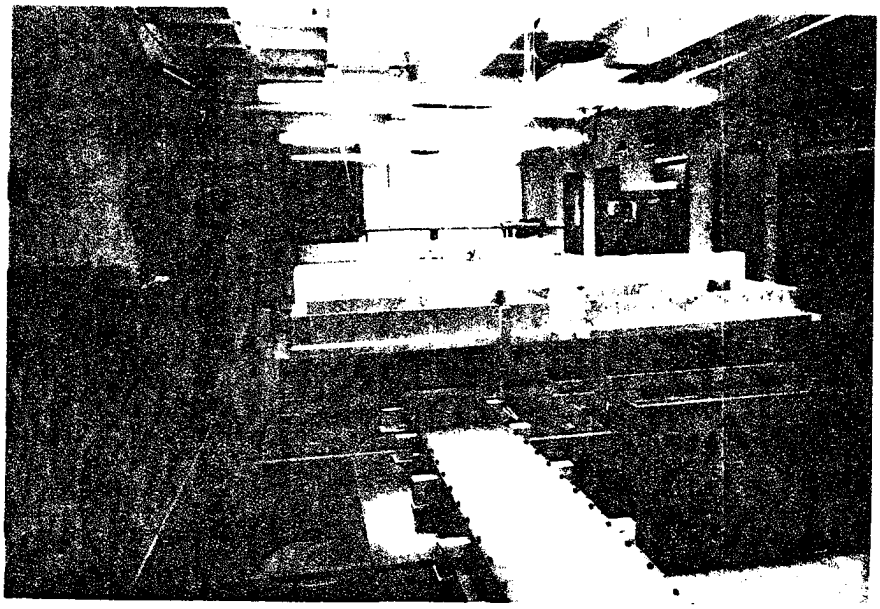

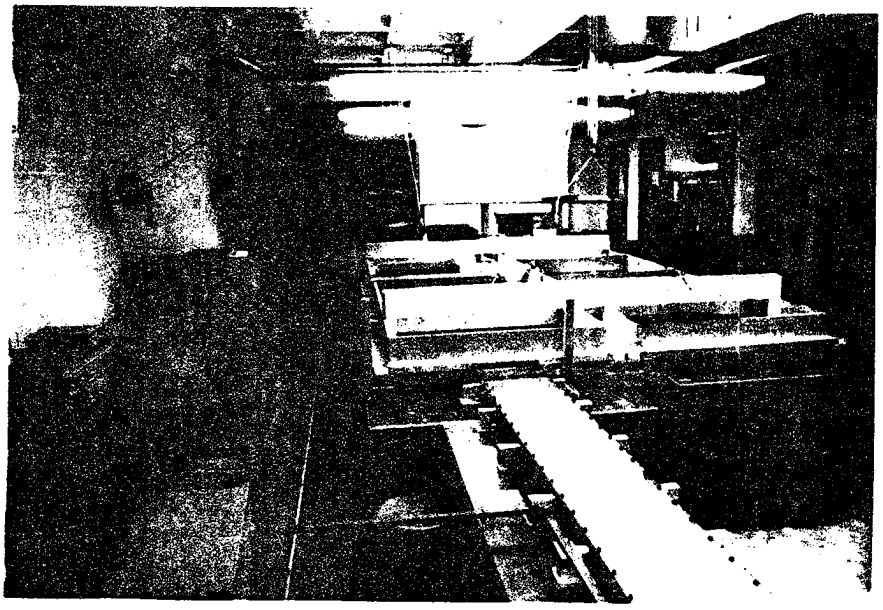

Fig. 6 Upper plate raised and lowered.

The horn used to excite the slab waveguide provided a gentle transition from an X-Band waveguide (1.0 cm by 2.3) cm to a multimode rectangular waveguide 13.7 cm by 1.0 cm into which a tapered piece of foam was inserted (Fig. 7). A cold rolled 1/4 inch thick steel drill template and number 46 drill were used to drill the measurement holes in the top plate. A great deal of care was taken to drill the holes accurately since the phase of the fields to be measured varies approximately 11 degrees/mm in the direction of propagation. Unused holes were covered with Scotch #431 aluminum tape. An FXR Model B200A probe with aluminum base (shown in Fig. 8) was inserted into the measurement holes to provide measurement of the transverse electric field inside and outside the slab waveguide. Emerson and Cuming Eccosorb LS-26, cut into wedges as shown in Fig. 9, was used to absorb the fields once they had propagated beyond the location of the measurement holes.

The measurement system is depicted in Fig. 10. A 9 GHZ sine wave modulated with a 1.7 KHZ square wave is generated by a FXR test oscillator, amplified by a Hewlett Packard (H.P.) power amplifier and fed to a (Cascade Research) Uniline isolator. Connection between these system elements is made with RG 9A/U coax. Directly connected to the output of the isolator is a (Sperry) Microline 20 db directional coupler whose primary output is connected, via X-Band waveguide, to the

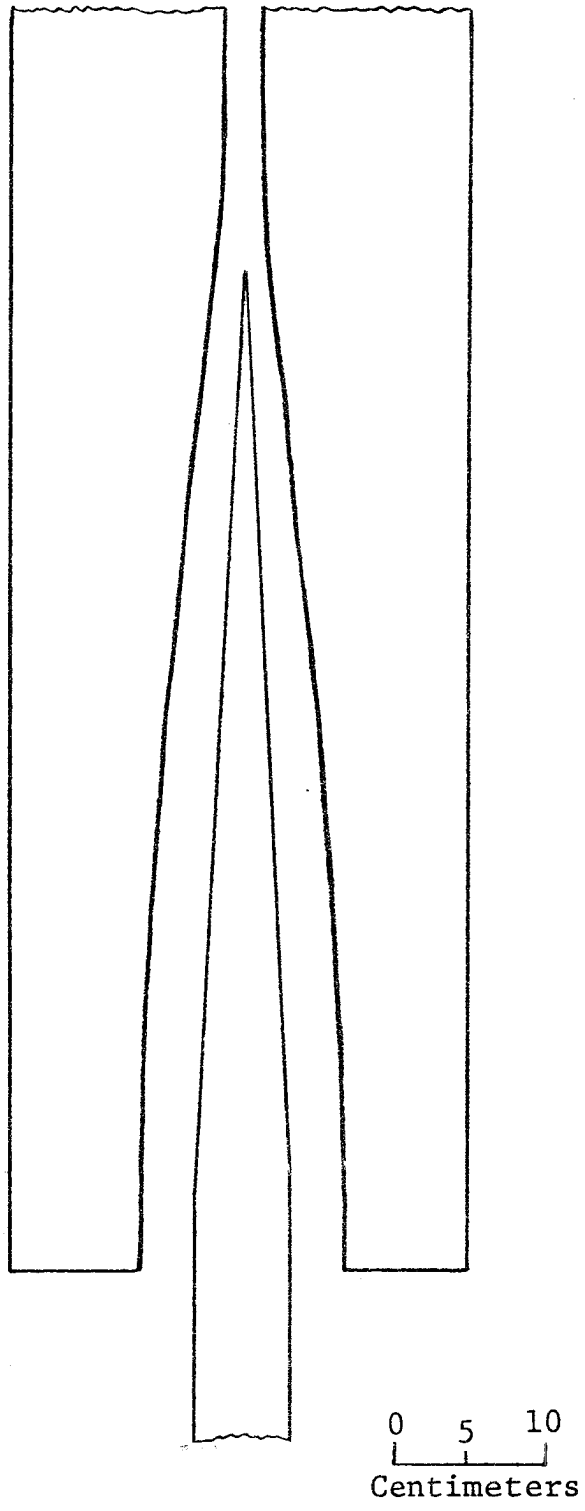

Fig. 7 Contour of horn used to excite slab waveguide.

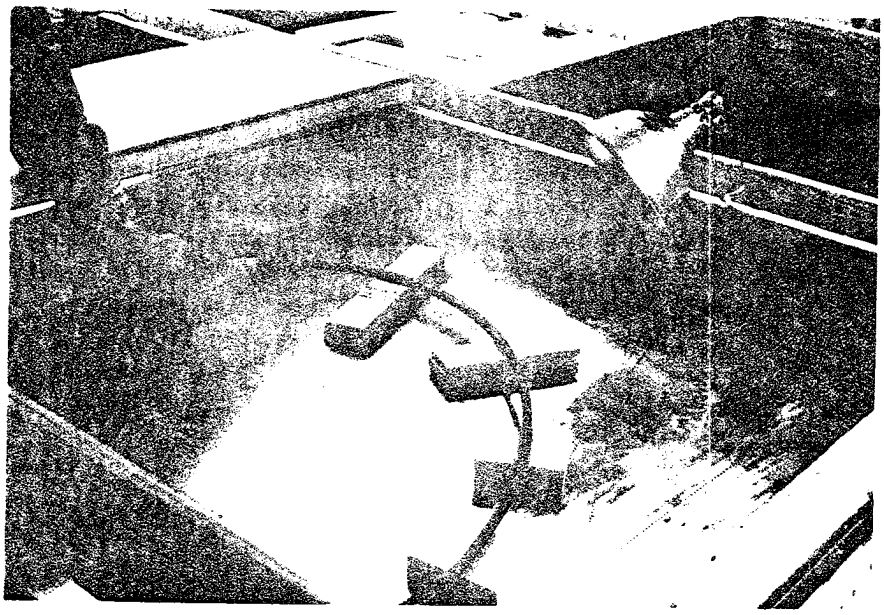

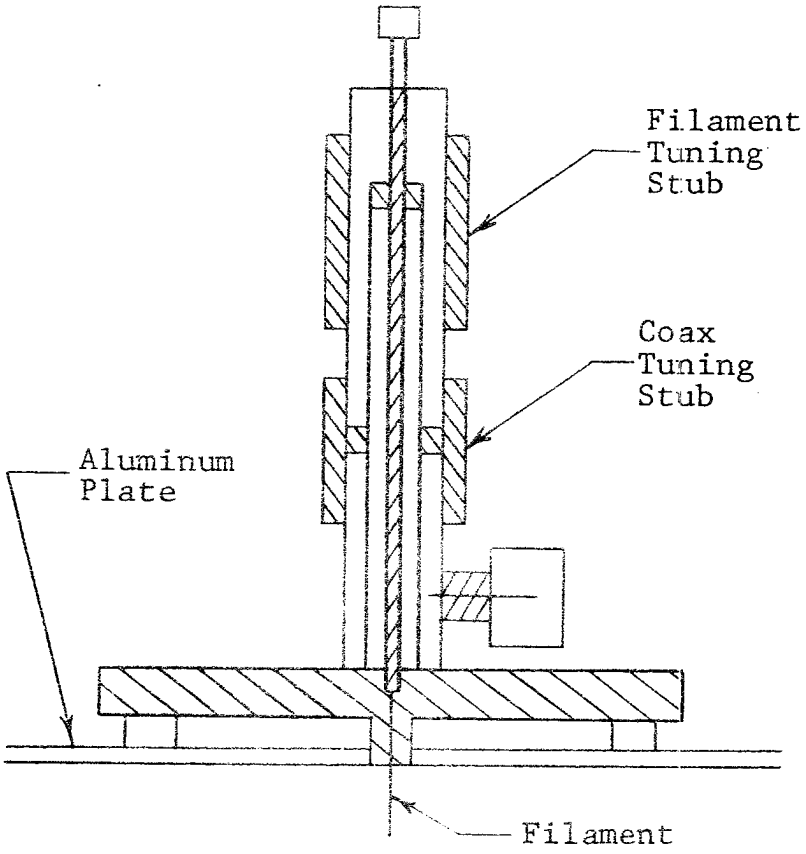

Fig. 8 Probe used to measure transverse electric field.

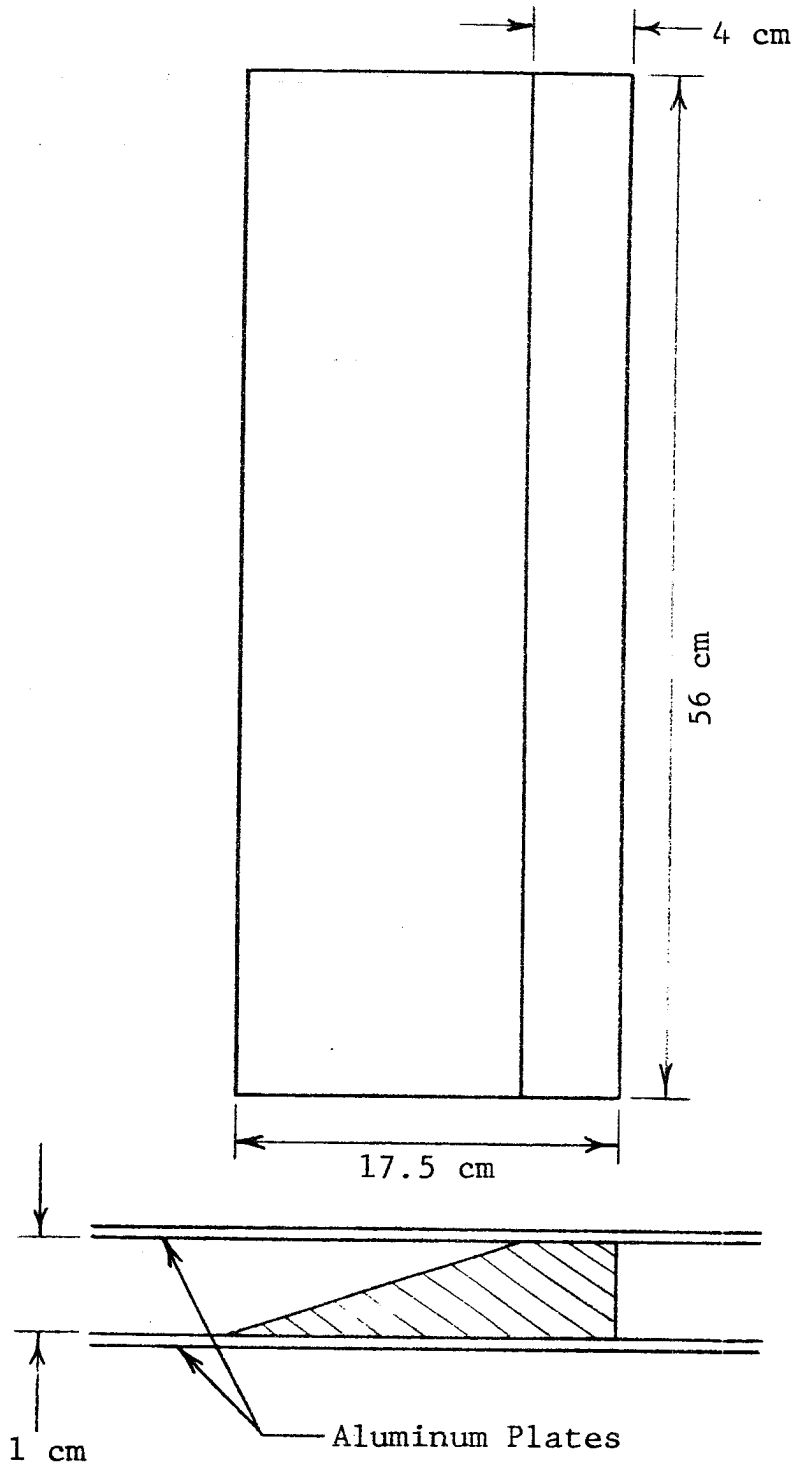

Fig. 9 Shape of absorber.

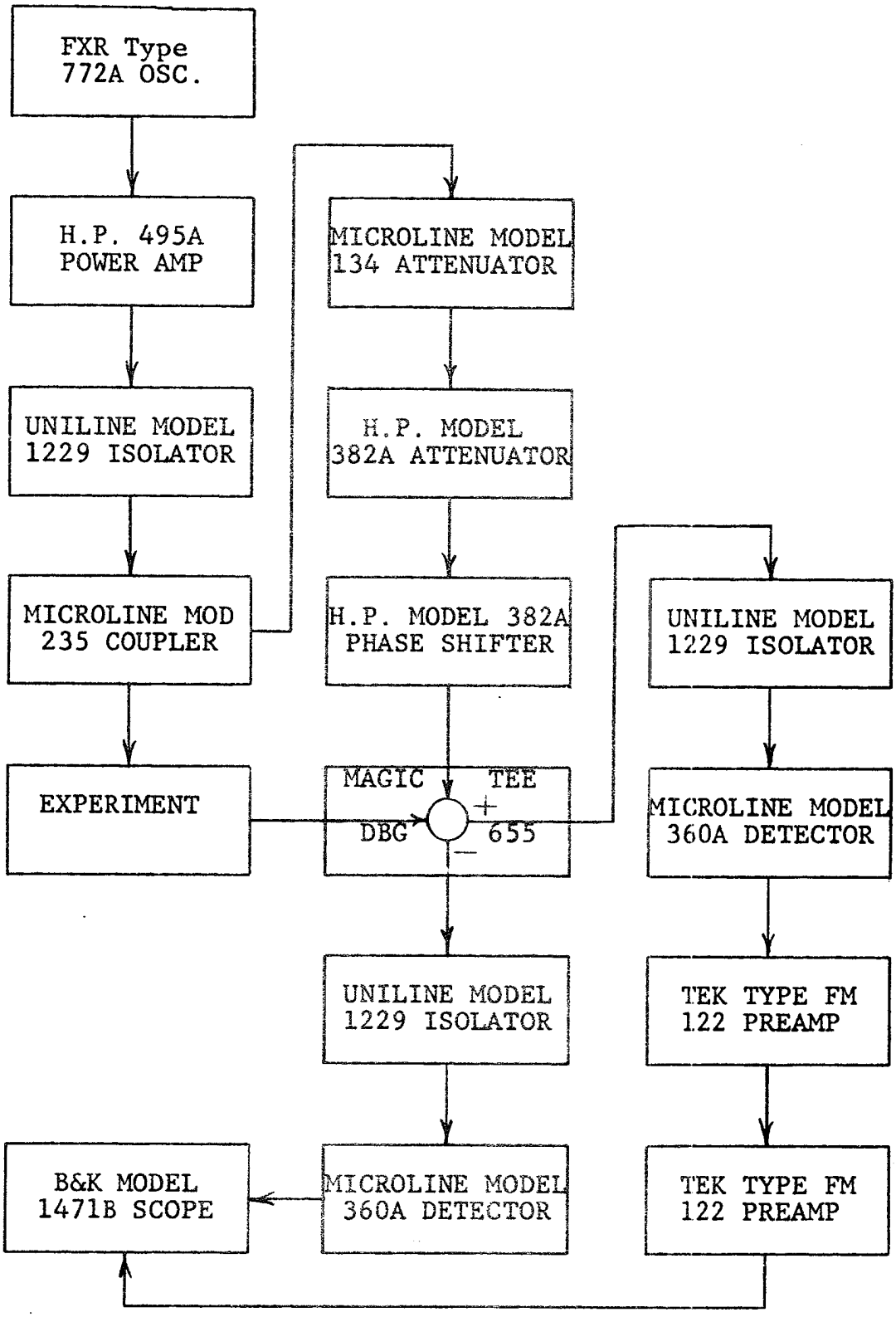

Fig. 10 Measurement system.

horn. The secondary output of the coupler is used as a reference signal and is fed through a Microline variable attenuator, an H.P. variable attenuator and an H.P. phase shifter to a DeMornay-Bonardi magic tee where it is added to the signal from the probe. Due to the directional characteristics of the coupler, signals reflected back into either of the coupler outputs are absorbed by the isolator. The coupler, two attenuators and phase shifter are connected directly while the phase shifter and the magic tee are connected with X-Band waveguide. All waveguide was securely bolted together and fastened to a sturdy bench to eliminate magnitude and phase errors caused by separation at the waveguide junctions. RG 9B/U coax provided the connection between the probe and the magic tee.

The sum of the reference signal and the probe signal is available at one magic tee output, while the difference is available at the other. Each of the output signals is fed through a Uniline isolator to a Microline crystal detector (tuned for maximum output) where it is demodulated. The detectors and isolators are directly connected to the magic tee. Signals reflected by the crystal detectors are absorbed by the isolators. The sum of the reference and probe signals is amplified by two Tektronix (Tek) low level preamplifiers and fed to channel A of a B&K oscilloscope. The preamplifiers are single-endedly connected in series with the first set for

a gain of 100 and the second for a gain of 1000. Channel B of the scope is connected to the other detector output. All connections between the scope and the detectors are made with RG 58/U coax.

When the H.P. variable attenuator (Microline variable attenuator remains set at 20 db) and phase shifter are adjusted such that the reference signal and probe signal are equal in magnitude and 180 degrees out of phase, a null will be observed on channel A of the scope. This null can be observed most easily when the scope is triggered externally with the test oscillator modulation signal, the modulation frequency is set to 1.7 KHZ and the preamplifier high pass and low pass filters are set to 10 KHZ and 80 HZ respectively. Once a null is obtained, a change in the magnitude and/or phase of the probe signal will cause an equivalent change in the settings of the attenuator and phase shifter (required to again obtain a null). This allows relative amplitude and phase measurements of the probe signal. Greater measurement accuracy is obtained as a direct result of the amplification provided by the preamplifiers. The signal observed on channel B of the scope is used to monitor the amplitude of the reference signal when the probe is disconnected and both attenuators are set to zero db (see TEST PROCEDURE).

All of the equipment is connected to a Weston-Rotek Model 150A regulator. Regulating the line voltage

increased the stability of the system and reduced conducted line noise seen on the scope.

CHAPTER IV

CALIBRATION

The first step of the system calibration was accomplished using an H.P. Model 809B slotted line, connected in place of the horn, with an H.P. Model 901B matched termination. To adjust the frequency of the test oscillator, an H.P. Model 532B frequency meter was connected between the test oscillator and the directional coupler. Maximum test oscillator output was obtained by adjusting the oscillator attenuator until the maximum output which yielded an accurate square wave was obtained.

The slotted line is equipped with a vernier probe position indicator that allows accurate short distance measurement (toward the termination) from an adjustable stop. With the probe filament extended 1 mm and the stubs tuned for the maximum output that would allow a null to be obtained (this level of probe output will be referred to as the level of maximum sensitivity), the location of the stop was then adjusted such that the phase shifter indicated zero degrees when the system was nulled. Using the vernier the probe was moved 0.1353 cm, the distance corresponding to a 10 degree phase shift in an X-Band waveguide. A null was obtained and the magnitude/phase readings recorded. After resetting the

vernier, the stop was readjusted to obtain a null at 10 degrees. The above procedure was repeated 35 more times and it was observed that the magnitude remained constant ± 0.1 db while the phase yielded the expected value ± 1.0 degree. This indicates that magnitude measurements ± 0.1 db and phase measurements ± 1.0 degree are possible when the system is operating at maximum sensitivity regardless of the reading on the phase shifter.

The purpose of the second step of the system calibration was to determine how the accuracy of the measurements decreased when the system was operated below maximum sensitivity. Repeated measurements were made at different magnitude levels until the range of error became identifiable. The results were as follows:

DB BELOW MAX. SENSITIVITY	MAGNITUDE ERROR	PHASE ERROR
0	± 0.1 DB	± 1 DEGREE
10	± 0.3 DB	± 2 DEGREES
20	± 0.5 DB	± 3 DEGREES
30	± 3.0 DB	± 12 DEGREES

The third step of the system calibration checked the calibration of the attenuator and verified that it did not introduce any variable phase shift. H.P. specifies that the Model X382A is accurate to ± 2% of the reading in db with no measurable phase shift. This accuracy was verified using H.P. Model 8491A 10 db and 20 db coaxial attenuators inserted between the probe and the magic tee for several levels of probe output. The resultant change in the magnitude and phase readings (insertion of the pad caused a constant phase shift independent of the magnitude reading) were better than expected considering the accuracy of the measurement system.

The final step of the system calibration tested two necessary properties of the measurement system. To verify that the probe did not disturb the field distribution being measured, a set of measurements was taken with the probe extended 2 mm, and then repeated with the probe extended 4 mm. The results were identical within the accuracy of the system. With the probe disconnected a metallic object was moved around inside the horn and the reference signal was viewed on the scope. Stability of this signal confirmed that signals reflected from the horn are not added to the reference signal, but absorbed by the isolator connected between the power amplifier and the coupler.

CHAPTER V

TEST PROCEDURE

The following procedure was used to obtain all of the experimental data presented in this thesis:

1. Check the flatness of the lower plates and make any necessary adjustments.
2. Remove adhesive on lower plate (using single edged razor blade) and lightly sand both plates (using a fine grade wet and dry sandpaper) to obtain a shiny surface.
3. Fasten the foam to the plates using 3M 77 spray adhesive. The adhesive must be sprayed onto a piece of paper, applied to the lower plate and allowed to dry for 15 minutes before contact is made with the foam.
4. Place absorbers and spacers on the lower plate such that a uniform separation between the plates will be obtained upon lowering the upper plate. Non-uniform separation on the order of several millimeters can cause substantial measurement error.
5. Allow the measurement system to warm up for one hour.

6. Measure and record amplitude of reference signal with probe disconnected and both attenuators set to zero db.
7. Measure and record the line voltage using an H.P. Model 403R RMS voltmeter.
8. Adjust probe so that the filament is extended 2 mm.
9. Set Model 134 attenuator to 20 db.
10. Insert probe into measurement hole corresponding to the maximum field strength to be measured and adjust it for maximum sensitivity.
11. Record measurement of maximum field strength.
12. Take desired measurements, making sure that probe cable is never sharply bent and probe is always firmly seated in the measurement hole, and record the data.
13. Measure and record maximum field strength. Compare these values to the previously recorded values to verify the stability of the test oscillator frequency.
14. Measure and record amplitude of reference signal. Compare these values to the previously recorded values to verify that the output of the H.P. power amplifier has remained constant.
15. Measure and record line voltage. Compare this value to the previously recorded value to verify the operation of the voltage regulator.

This procedure yielded very accurate and repeatable results as will be seen from the data exhibited in the following chapters.

CHAPTER VI

SINGLE MODE DIELECTRIC SLAB WAVEGUIDE

This phase of the project was begun by selecting a slab width of 7.6 cm (TE_1 mode will not propagate if $\varepsilon_r < 1.048$) based upon the guess that ε_r was approximately 1.040 for the polyethylene foam being used. A piece of foam aproximately 336 cm in length, with two pieces of absorber positioned directly at the end of the foam, was placed between the plates to model a single mode dielectric slab waveguide. Once it was verified that a surface wave could be excited (see Fig. 11), several sets of longitudinal measurements along the slab were made. Using the least squares method, a straight line was fitted to the phase data points, the slope of which was used to determine ε_r. These experiments yielded the following results:

1. Consistent magnitude errors of ± 0.4 db seemed to be caused by imperfections in the foam.
2. Minimizing the amount of surface wave reflected by the absorber resulted in a smaller range of ε_r.
3. Shortening the slab by 8.3 mm changed the calculated value of ε_r from 1.046 to 1.050.

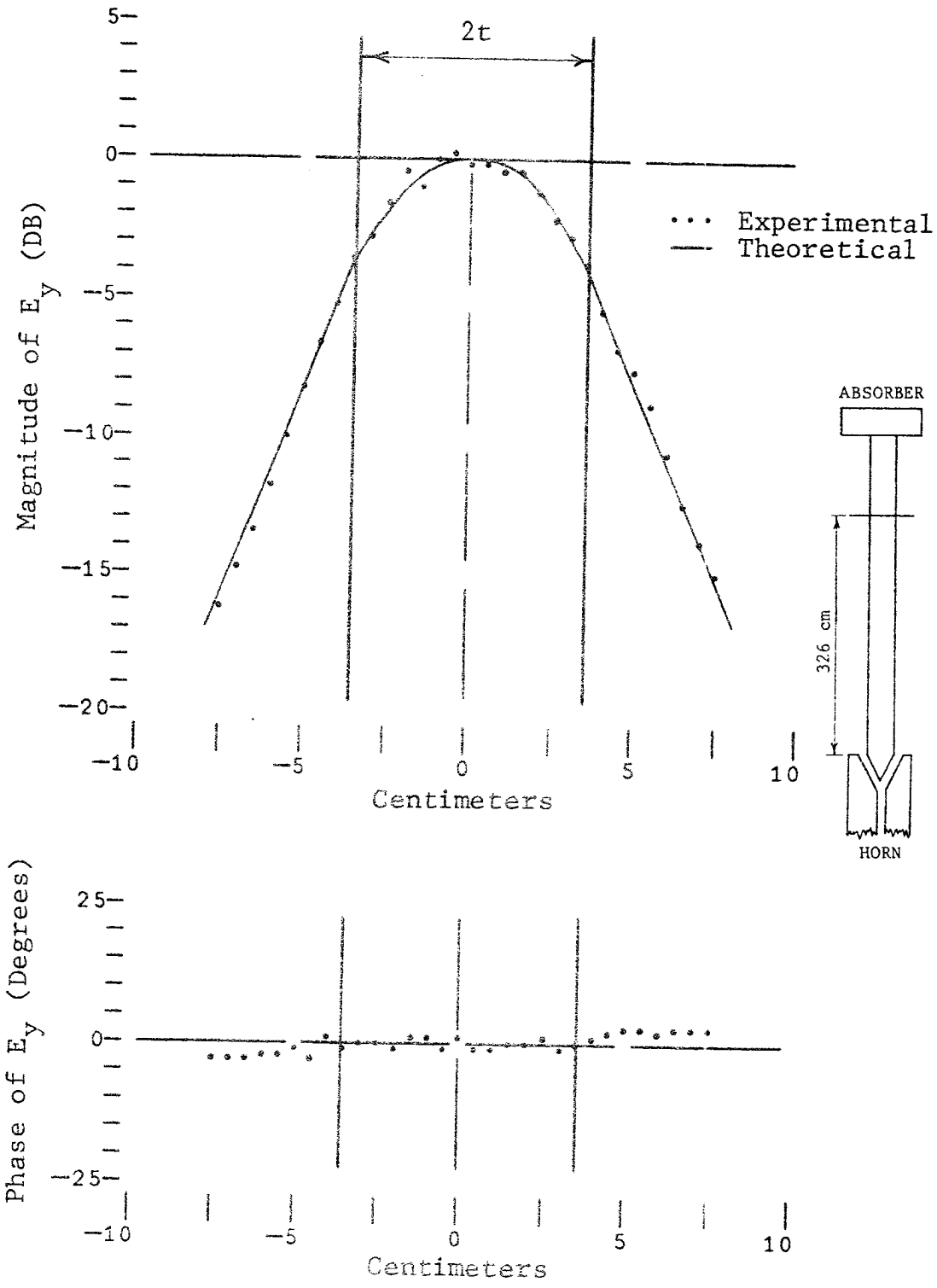

Fig. 11 Typical surface wave 326 cm from horn. Slab width (2t) = 6.5 cm = 1.95 λ.

4. Values of ε_r greater than 1.048 were obtained indicating that the slab width must be decreased if single mode operation was to be insured.

A new slab width of 6.5 cm (TE_1 mode will not propagate if $\varepsilon_r < 1.066$) was then chosen and the longitudinal measurements were repeated four times with the slab shortened 3 mm for each experiment. Values of $\varepsilon_r = 1.05 \pm 0.006$ were subsequently obtained and used to generate the theoretical curve for comparison to the experimental data in Fig. 11.

While the measured data exhibits excellent agreement with theory, the measurements were taken at the extreme end of the plates where radiation from the horn is minimal. Since the experiments described in the following chapters involve surface wave measurements 127 cm and 202 cm from the horn, measurements taken at these locations are shown in Fig. 12 for a 6.5 cm slab. Note that these measurements were taken over 20.5 cm instead of 15.5 cm as in Fig. 11.

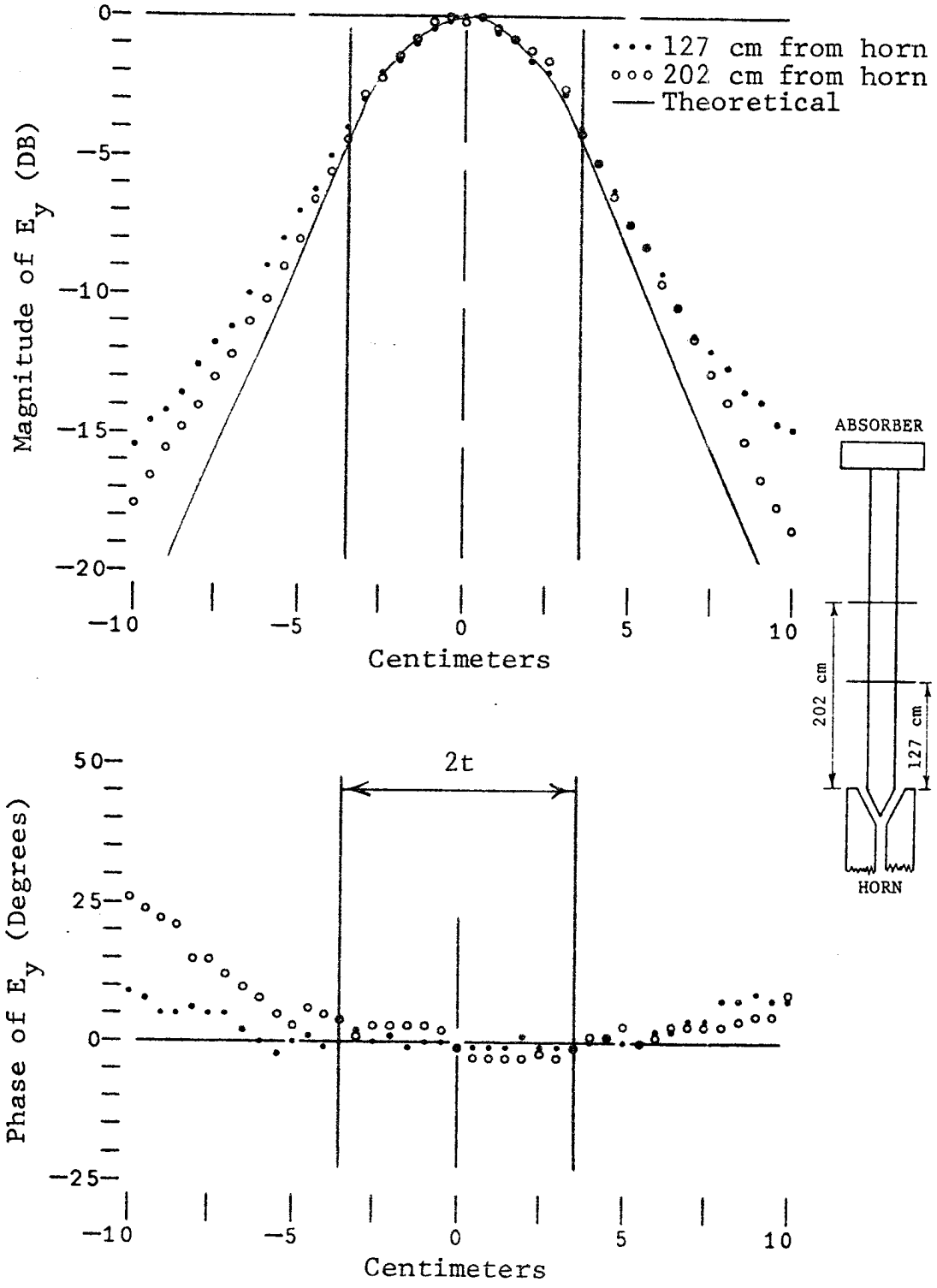

Fig. 12 Surface wave 127 cm and 202 cm from horn. Slab width (2t) = 6.5 cm = 1.95λ.

CHAPTER VII

RADIATION FROM THE END OF A SINGLE MODE DIELECTRIC SLAB WAVEGUIDE

To obtain the radiation pattern of truncated and angled end single mode dielectric slab waveguides, measurements were taken along a 40 cm radius centered at the middle of the waveguide ends. The foam used to model the waveguide was 6.5 cm wide and 127 cm in length. Four absorbers were placed outside the radius to prevent the radiated fields from being reflected by the edge of the conducting plates.

The radiation pattern for a truncated slab is shown in Fig. 13. The theoretical pattern in Fig. 13 was obtained by substituting (2-31) into (2-32) with $\varepsilon_r = 1.05$, $k = 0.6\pi$ cm^{-1} (the values of h,p and β were the same as the ones used to generate the theoretical surafce wave plot in Fig. 12). Experimental and theoretical radiation patterns show fair agreement over the majority of the main lobe. The discrepancy between theoretical and experimental radiation patterns as well as the corresponding progressing phase are the result of measurements being made in the Fresnel zone. Calculation of the fields in this zone requires a more refined analysis as presented in Jordan and Balmain [13].

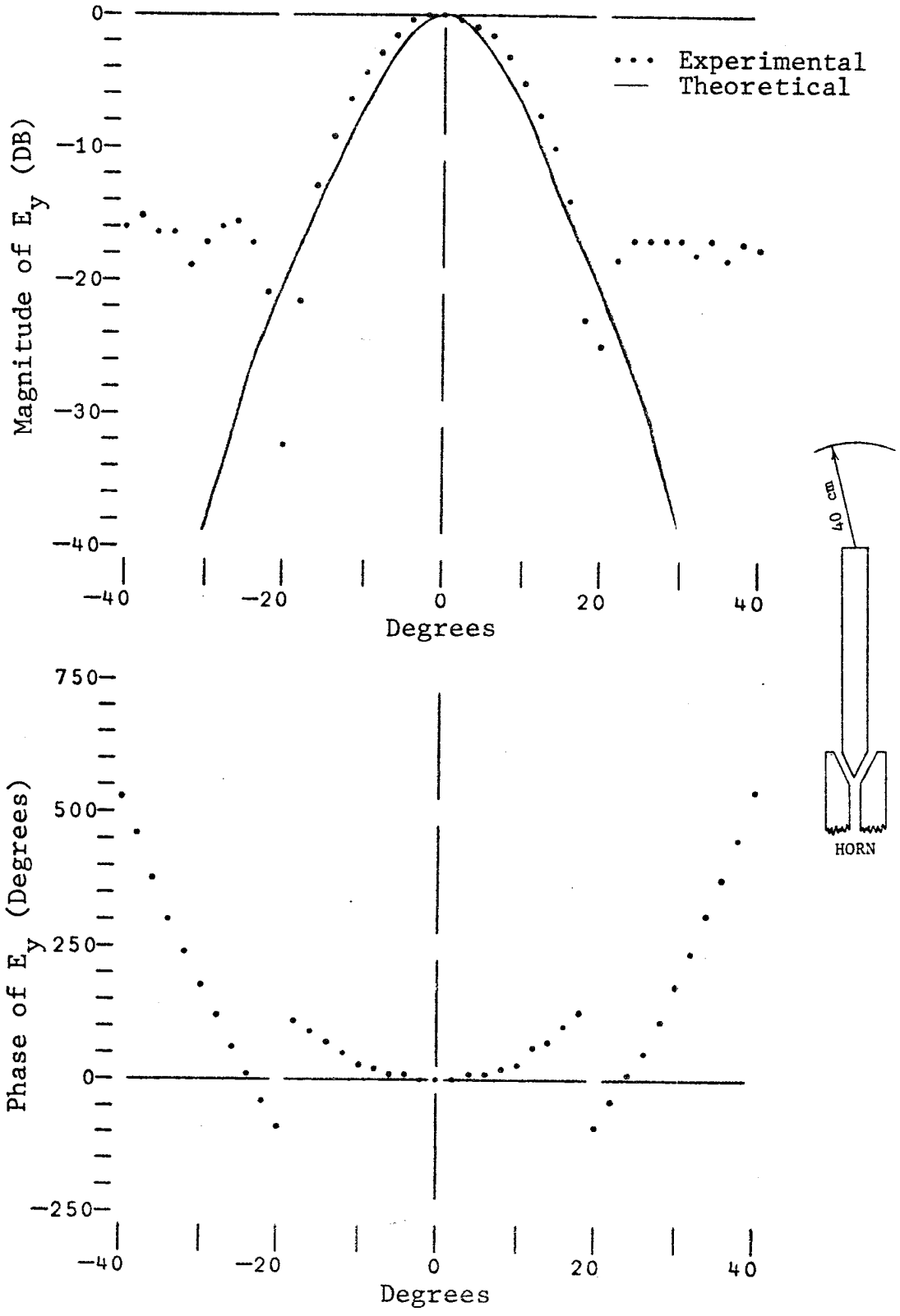

Fig. 13 Radiation pattern of a truncated waveguide.

Fig. 14 exhibits the radiation patterns for 30 degree and 10 degree angled ends. In each case the location of the angle tip corresponded to the previous position of the corner of the truncated slab. Comparing Fig. 14 with Fig. 13 one can see that decreasing the angle of the end (the truncated slab is assumed to have a 90 degree angled end) causes a slight broadening of the main lobe as well as a considerable change in the magnitude and phase of the side lobes. The radiation pattern for the 10 degree angled end was also obtained with the end advanced 18.4 cm (1/2 the length of the angle) and is shown in Fig. 15. The radiation pattern for the 10 degree angled end shown in Fig. 14 is also presented in Fig. 15 for comparison purposes. Moving the end forward caused a narrowing of the main lobe making it appear that the phase center is located at the end of the angled section.

Measurements of the surface wave travelling along 30 degree and 10 degree angled ends are displayed in Figs. 16 and 17. These plots show that the effect of the angled end is to pull the surface wave toward the location of the foam.

Longitudinal measurements along the slabs showed no measurable standing wave indicating that the reflection coefficient for both the truncated or angled end slabs is quite small as expected.

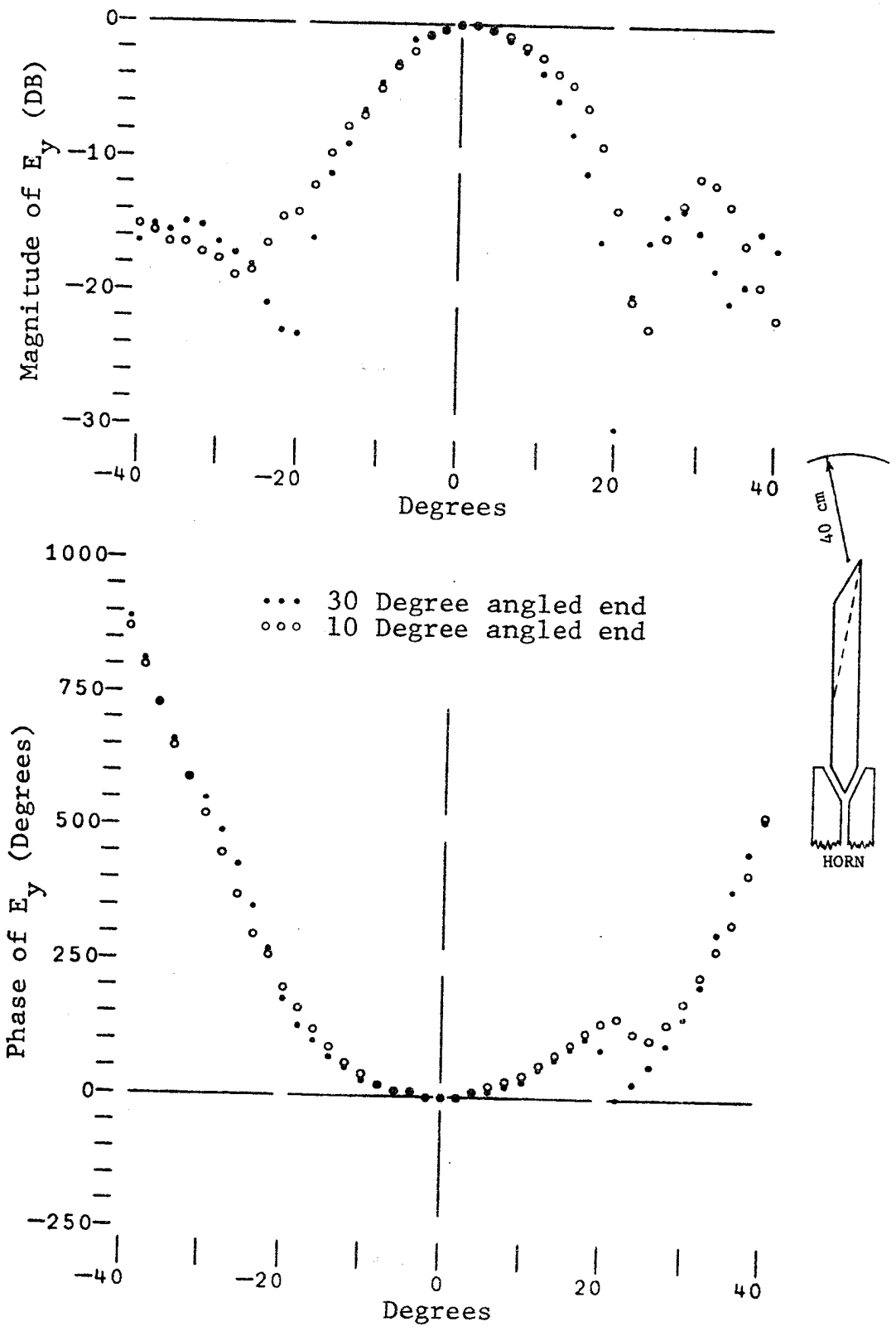

Fig. 14 Radiation patterns of angled end waveguides.

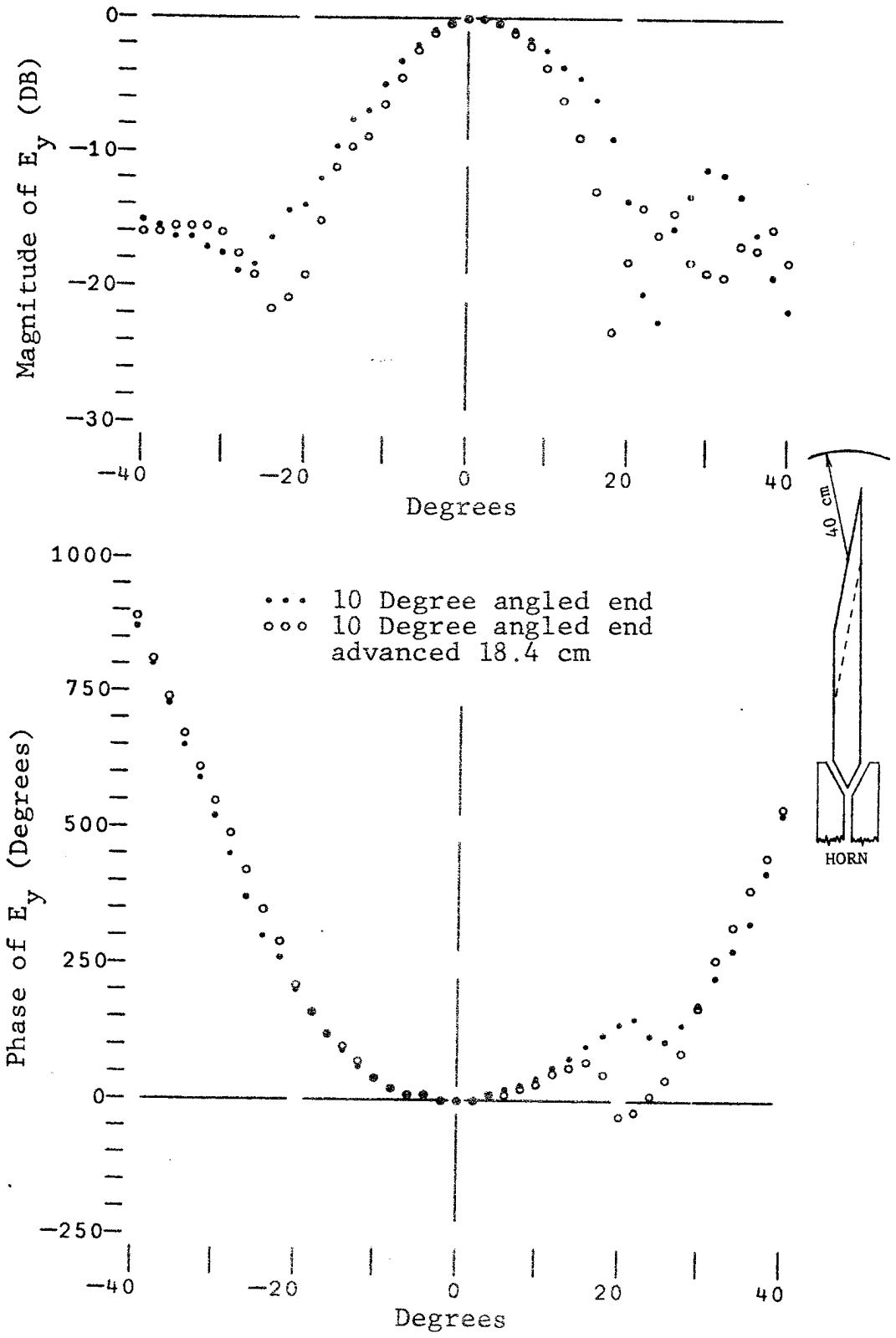

Fig. 15 Effect of advancing a 10 degree angled end.

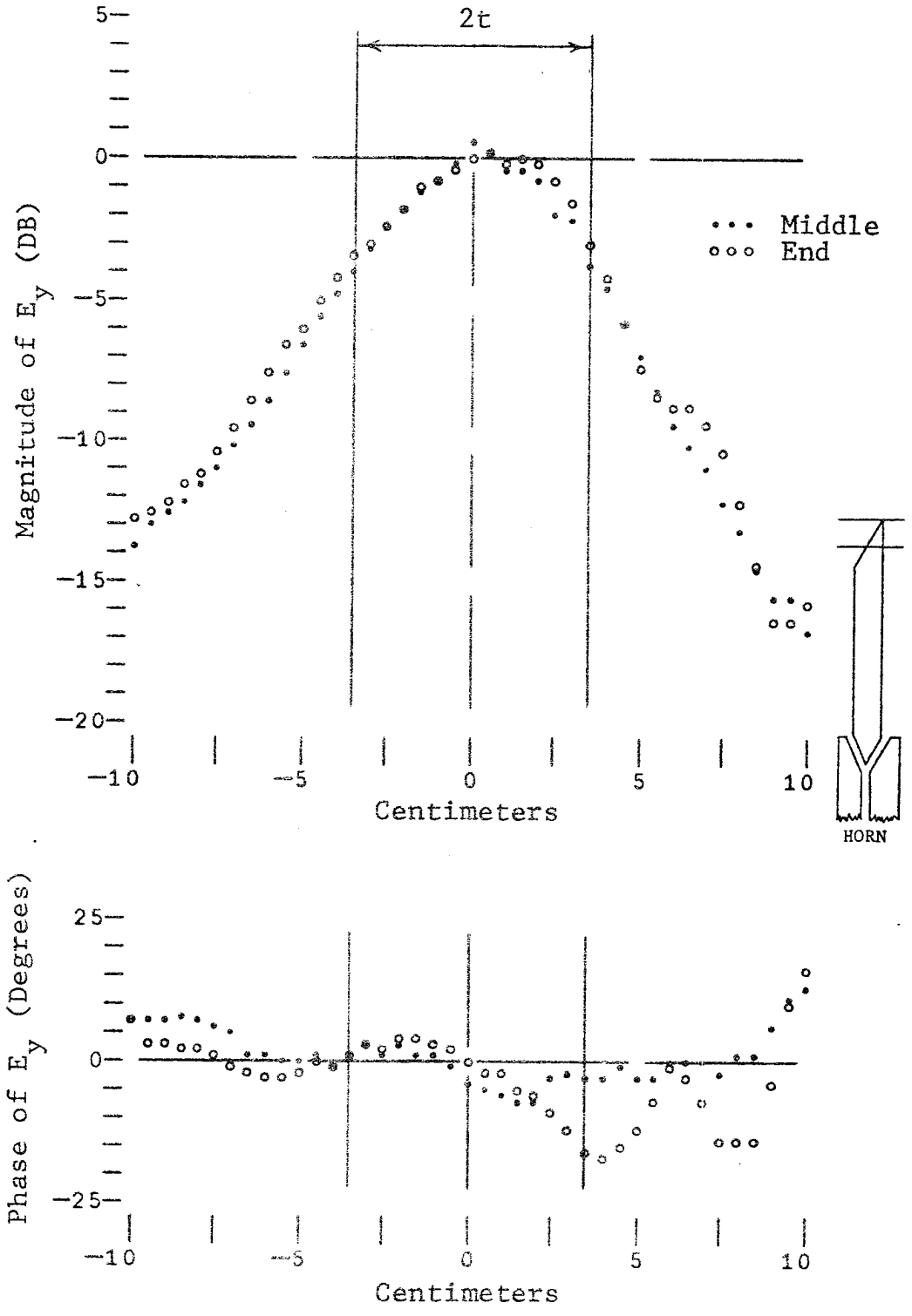

Fig. 16 Surface wave travelling along a 30 degree angle. Slab width (2t) = 6.5 cm = 1.95 λ.

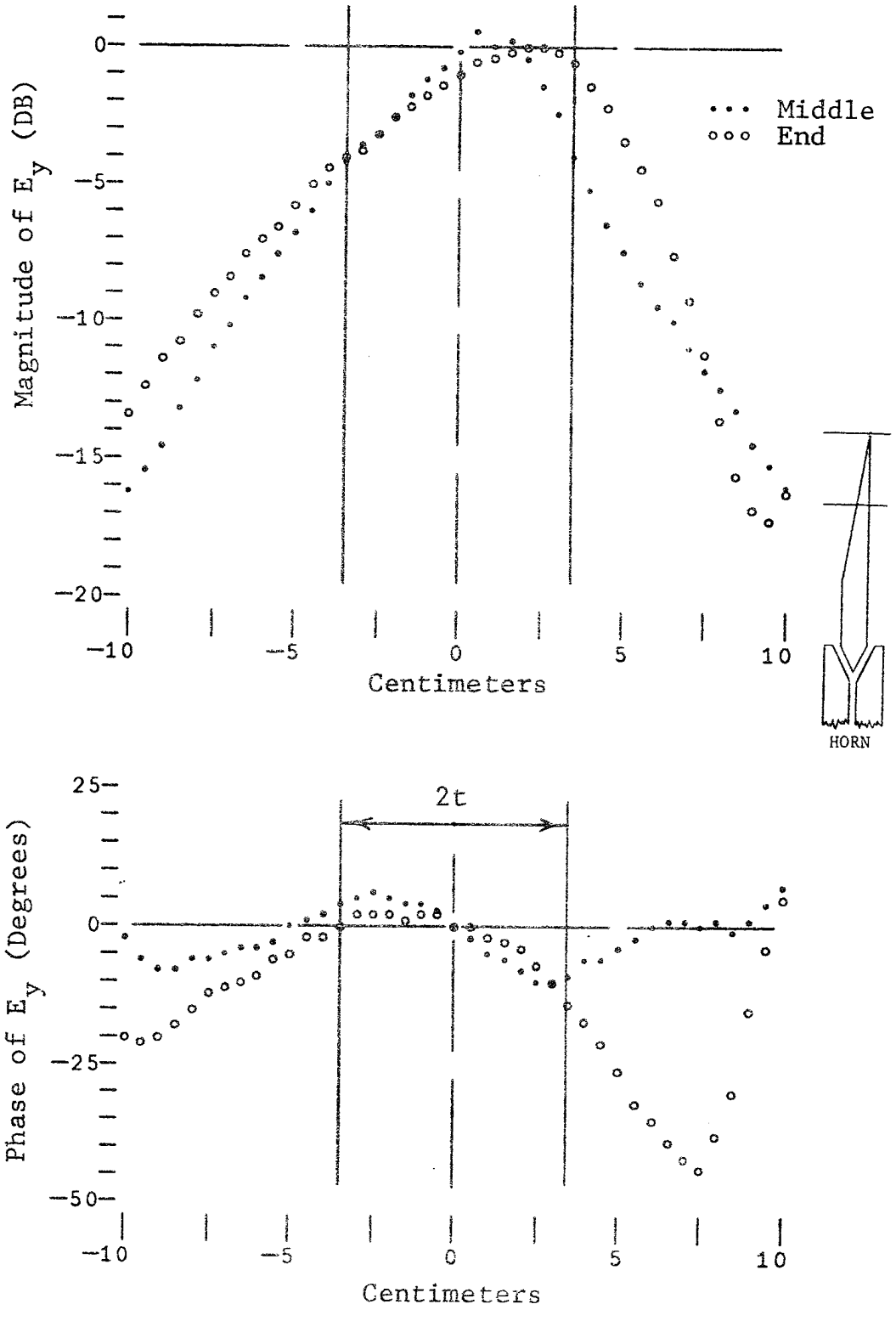

Fig. 17 Surface wave travelling along a 10 degree angle. Slab width (2t) = 6.5 cm = 1.95λ.

CHAPTER VIII

GAPS AND OFFSETS IN A SINGLE MODE DIELECTRIC SLAB WAVEGUIDE

The final phase of the project consisted of determining the effect of gaps and/or offsets between sections of single mode dielectric slab waveguides having truncated and 30 degree angled ends.

Transverse magnitude and phase measurements were made across the receiving slab 172 cm from the horn. To minimize the effect of local radiation (if any exists), the end of the truncated transmitting slab was positioned 3 cm beyond the measurement holes. The tip of the angled end transmitting slab did not extend beyond the location of the measurement holes. Two absorbers were used to terminate the receiving slab and one absorber was placed on each side of the receiving slab to absorb radiation from the gaps and/or offsets.

The magnitude measurements were normalized by the maximum amplitude of the surface wave on the transmitting slab 127 cm from the horn. Phase measurements on the receiving slab are referenced to the phase of this maximum amplitude. With a continuous slab installed, the magnitude of the surface wave was found to be 0.5 db greater at the receiving slab than it was at the transmitting slab. Because this discrepancy was

attributed to a small non-uniformity in plate separation, a 0.5 db correction factor was added to the magnitude of the surface wave on the transmitting slab.

The results of 10 cm, 20 cm and 30 cm gaps between truncated sections is presented in Fig. 18. One can see the decreasing attenuation of the maximum magnitude of the surface wave caused by 10 cm increments in the gap size. This is consistent with the results of Neumann [4] for a microwave model of a single-mode fiber. From Fig. 19 it can be seen that 0 cm, 10 cm and 20 cm gaps combined with a 5 cm gap exhibit a similar effect as might be expected. a 20 cm gap are shown in Fig. 20. This figure shows that reversing the angled face does not change the coupling significantly. Comparison with Fig. 20 shows that a 20 cm gap between 30 degree angled end sections has approximately the same attenuation effect as a 20 cm gap between truncated sections.

Fig. 21 contains the results of a 20 cm gap combined with a 5 cm offset between 30 degree angled end sections. These results show that for a constant gap and offset, the smaller the distance between the tips, the less the attenuation that is observed. This result agrees with what one might expect if the results of the previous chapter are considered.

Measurements made with the receiving slab removed (both truncated and angled ends) are shown in Fig. 22.

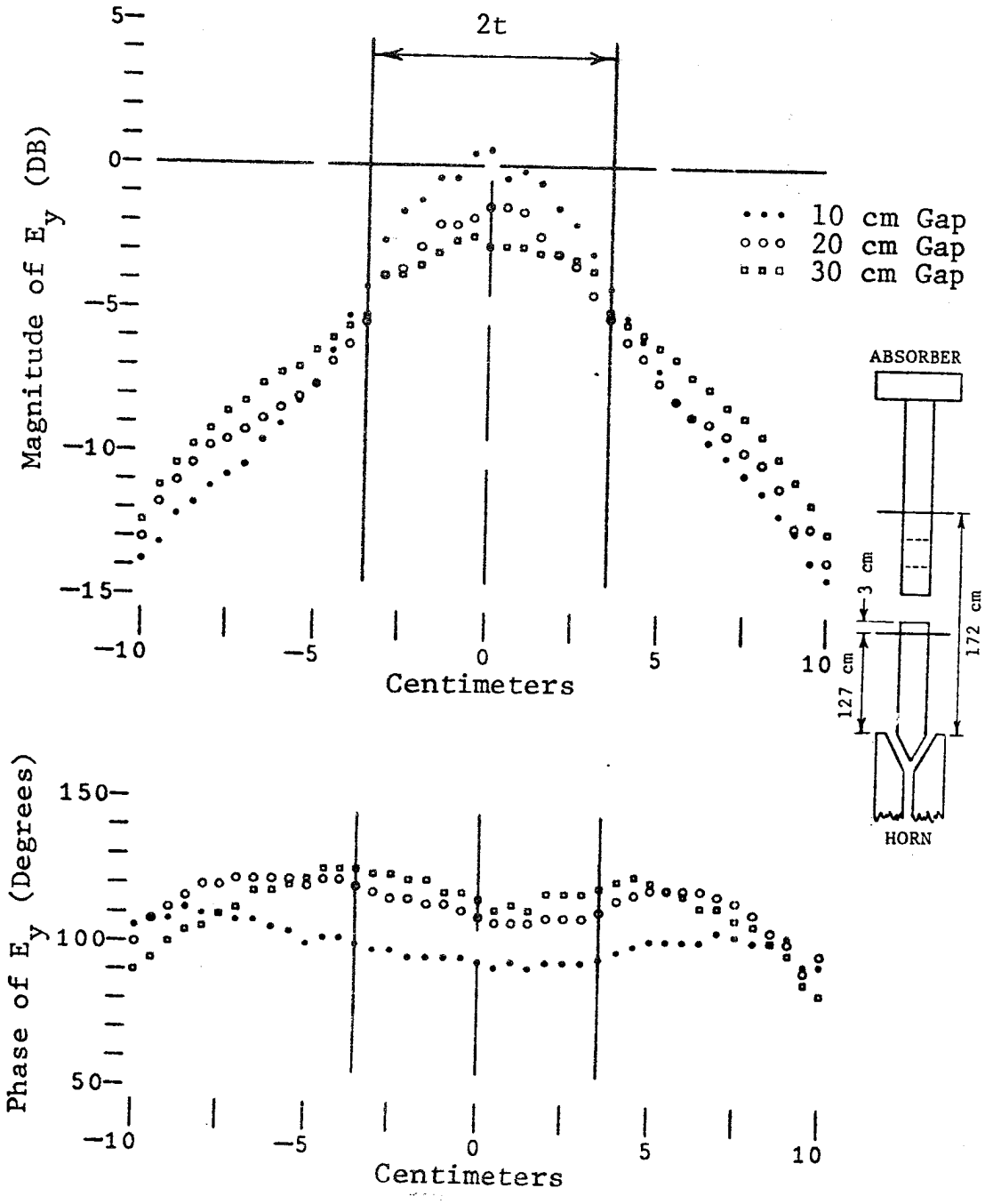

Fig. 18 Gaps between truncated waveguide sections. Slab width (2t) = 6.5 cm = 1.95λ.

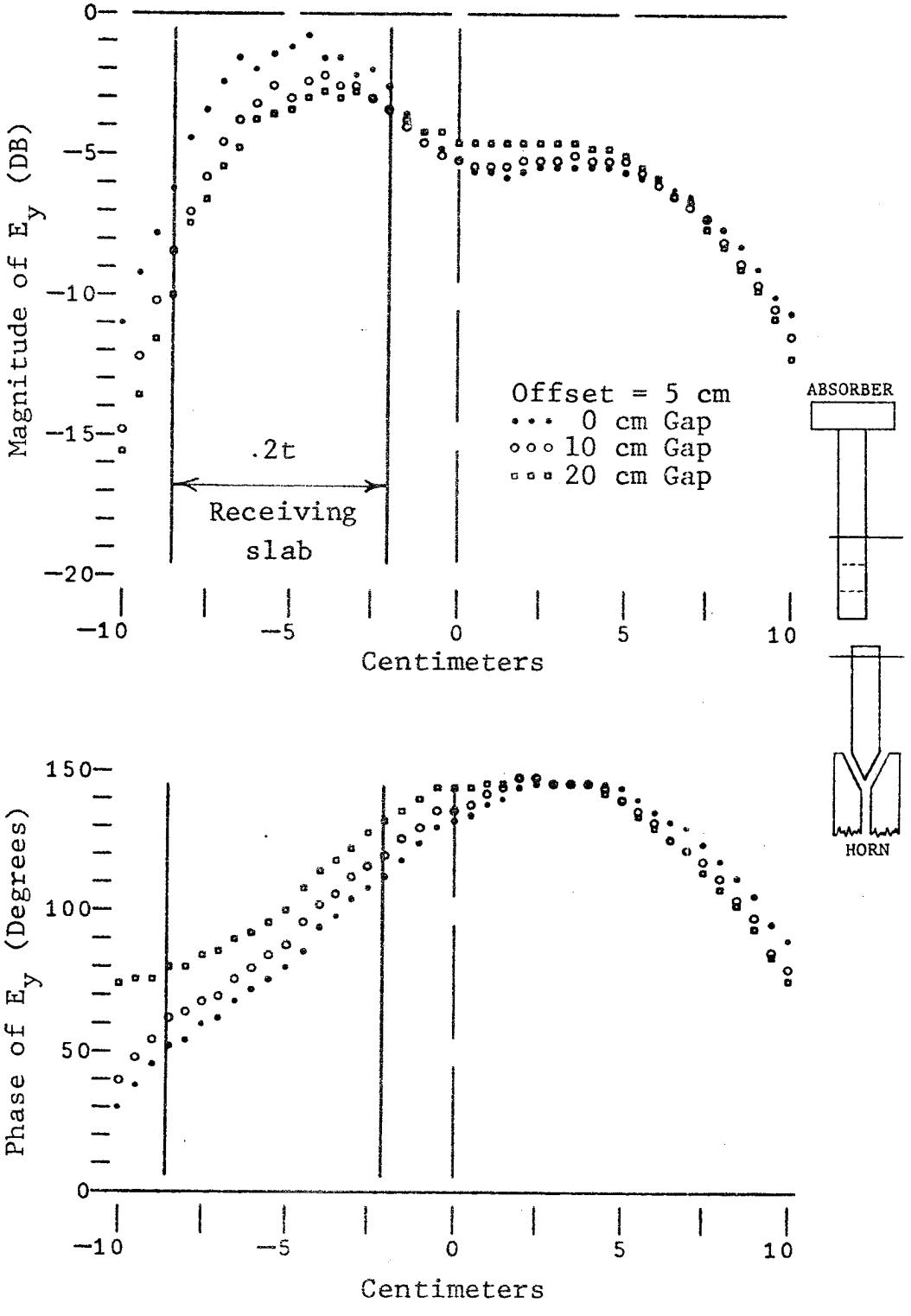

Fig. 19 Gaps and offset between truncated sections. Slab width (2t) = 6.5 cm = 1.95λ.

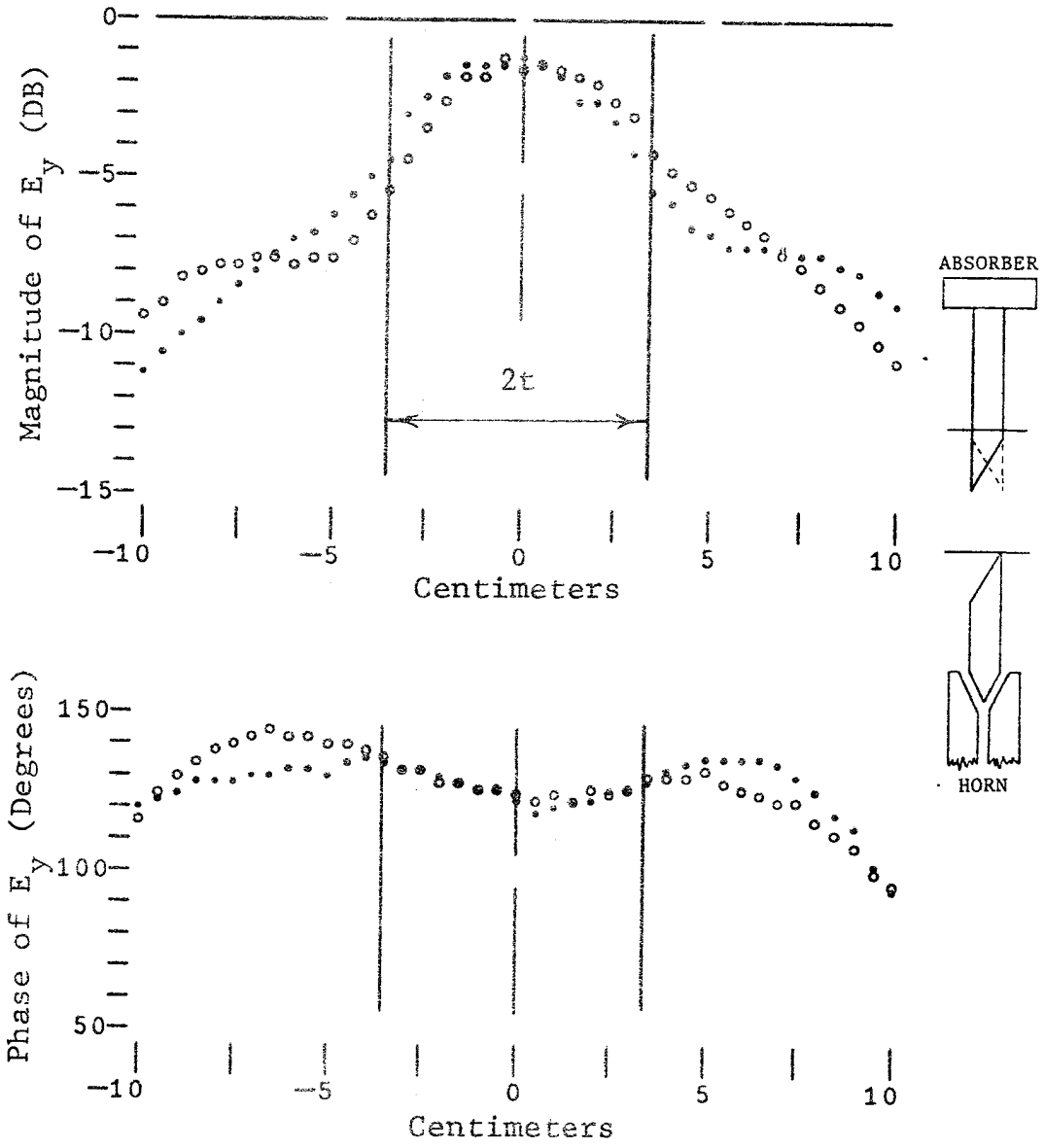

Fig. 20 Gap between 30 degree angled end sections. Slab width (2t) = 6.5 cm = 1.95λ.

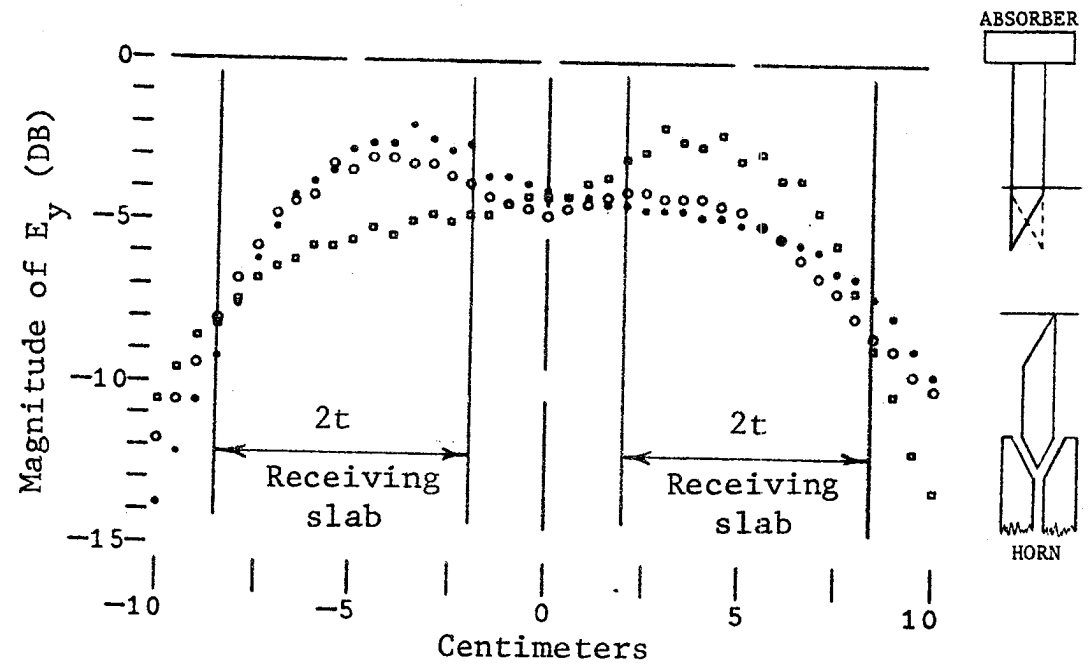

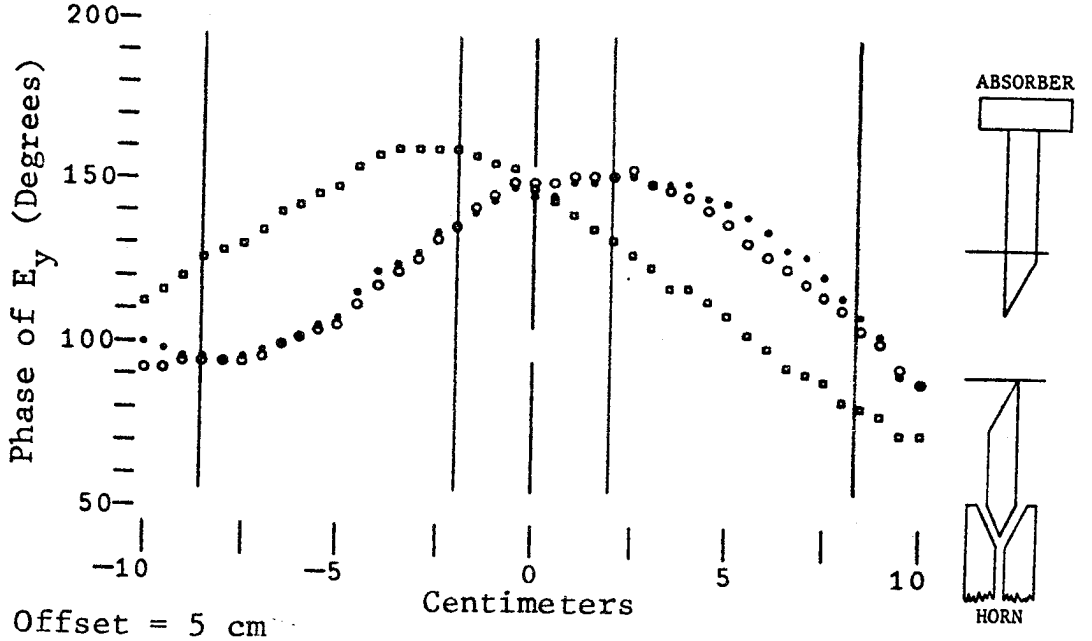

Offset = 5 cm
••• Reversed angle faces
ooo Parallel angle faces offset to left
▫▫▫ Parallel angle faces offset to right

Fig. 21 Gap and offset between angled end sections. Slab width (2t) = 6.5 cm = 1.95λ.

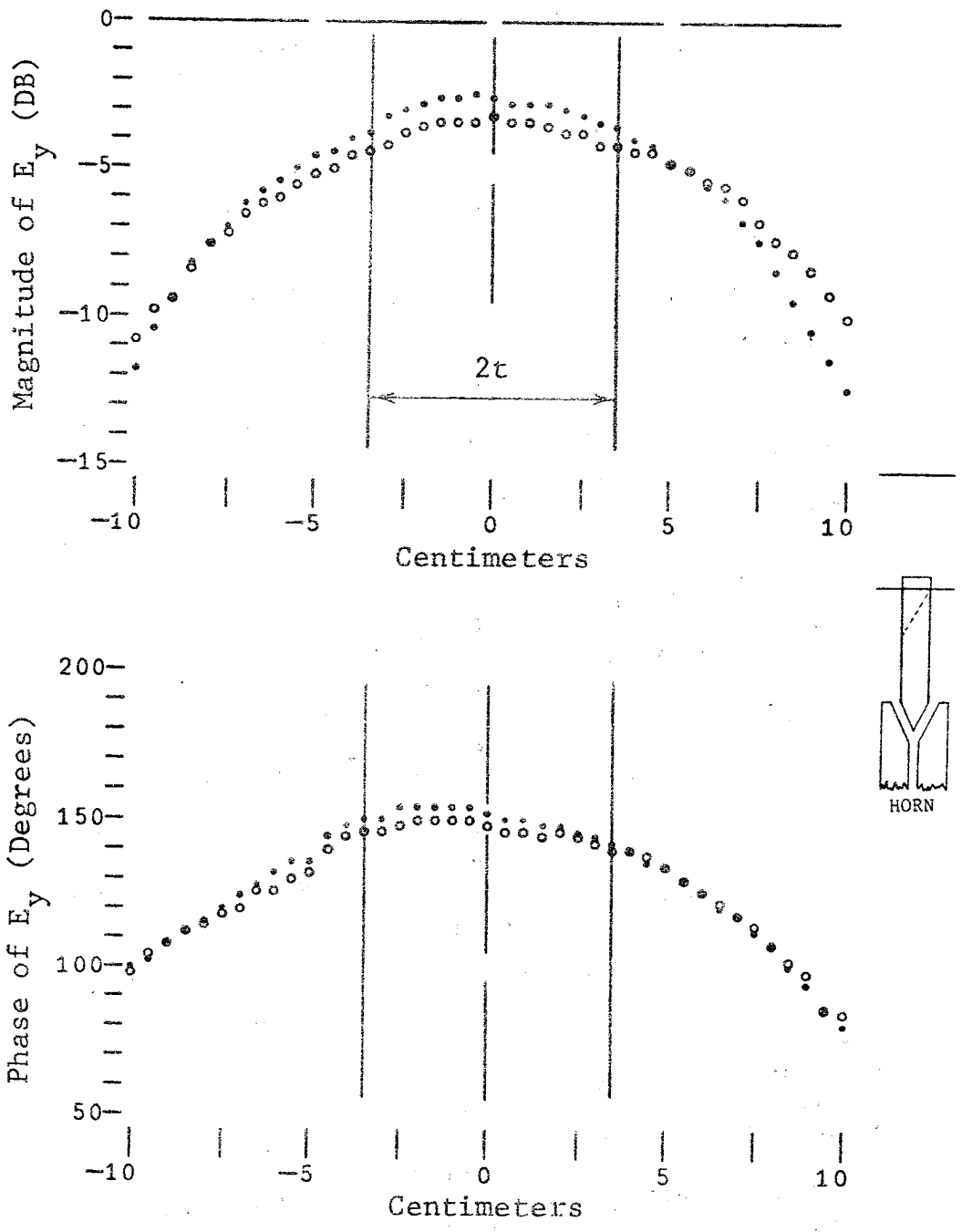

Fig. 22 Fields measured with receiving slab removed. Slab width (2t) = 6.5 cm = 1.95 λ.

CHAPTER IX

CONCLUSION

The experimental technique used to obtain the data presented in this thesis provided accurate and repeatable measurements as desired. However, radiation from the horn did have an undesirable effect upon the experimental data. Since no attempt was made to optimize the taper of the horn, alternate tapers should be explored by anyone planning to use this model in the future.

Maintaining a constant separation between the plates is a problem that was overcome, but only with a great deal of time and effort. The difficultly encountered was that the wooden tables and plywood frame expanded and contracted as the humidity in the room varied, requiring the plates to be leveled before each experiment. Use of an all metal structure would greatly reduce the amount of time necessary to conduct an experiment.

Measurements taken in the slab exhibited magnitude errors of less than ± 0.5 db. It is suspected that these errors are a result of non-uniformities in the foam. While this error is certainly not large, it could possibly be eliminated using a different type of foam.

The experimental data indicates that the effect of an angled slab waveguide end is to pull the surface wave toward the location of the dielectric. This mechanism

also became apparent in the investigation of a 20 cm gap combined with a 5 cm offset between sections having 30 degree angled ends. It was observed that for a constant size gap and offset, the smaller the distance between the tips, the larger the amplitude of the surface wave on the receiving slab.

The results of this thesis should be useful in both optical fiber and integrated optic applications. With an understanding of the angled end, fiber splices can now be designed to make use of such an effect. Integrated optic devices such as switches, modulators and directional couplers can be developed using the angled end effect to improve overall performance. Future theoretical research should also be motivated by the angled end mechanism.

REFERENCES

[1] D. Gloge, Optical Fiber Technology. New York: IEEE press, 1976.

[2] D. Marcuse, "Loss analysis of single mode fiber splices," The Bell System Technical Journal, Vol. 56, No. 5, May-June 1977.

[3] B. Rulf, "On matching two optical waveguides," Radio Science, Vol. 12, No.4, pp 593-601, July-August 1977.

[4] E.G. Neumann, "Inhomogeneities in monomode optical waveguides," Nouvelle Revue d'Optique, t. 6, No. 5, pp 263-271, 1975.

[5] J. Albrecht and E.G. Neumann, "Simulation of the near field of single-mode fibers by means of a microwave model, Microwaves, Optics and Acoustics, Vol. 3, No.3, p. 109, May 1979

[6] Bisbee, D.L., "Measurements of loss due to offsets and end separations of optical fibers," The Bell System Technical Journal, Vol. 50, pp. 3153-3158, December 1971.

[7] D. Marcuse, Integrated Optics. New York: IEEE press 1973.

[8] D. Marcuse, Light Transmission Optics. New York: Van Nostrand Reinhold, Chapter 8, 1972.

[9] Bahar, E., "Inhomogeneous dielectric filling to simulate curvature in a model earth-ionosphere waveguide," Proceedings of the IEE (London), Vol. 116, No. 1, January 1969.

[10] Haddad, H.A., "Microwave model study of an optical dielectric slab waveguide," Masters Thesis, University of Colorado, 1975.

[11] V.V. Shevchenko, Continuous Transitions in Open Waveguides. Colorado: Golem Press, 1971.

[12] L. Lewin, "Method for the calculation of the radiation-pattern and mode-conversion properties of a solid-state hetrojunction laser," IEEE Transactions on Microwave Theory and Techniques, Vol. 23, No. 7, p 576, July 1975.

[13] E.C. Jordan and K.G. Balmain, Electromagnetic Waves and Radiating Systems. New Jersey: Prentice Hall, pp. 498-503, 1968.